

The Arroyo Rojo volcanic-hosted massive sulphide deposit (Tierra del Fuego, southernmost Argentina): geology, mineralogy, petrography and mineral chemistry

Cecilia Biel¹, Ignacio Subías^{1,*}, Isabel Fanlo, Ester Mateo¹, and Rogelio Daniel Acevedo²

¹ Grupo de Recursos Minerales, Dpto. Ciencias de la Tierra, Universidad de Zaragoza,
Edificio Geológicas, c/Pedro Cerbuna, 12, Zaragoza 50009, España.

² Centro Austral de Investigaciones Científicas (C.A.D.I.C.),
Bernardo Houssay, 200, V9410CAB Ushuaia, Tierra del Fuego, Argentina.

* isubias@unizar.es

ABSTRACT

The Arroyo Rojo deposit is the most important polymetallic, volcanic-hosted massive sulphide close to the town of Ushuaia in the rhyolitic belt of the Andes of the Tierra del Fuego. The deposit occurs in a region with north-verging thrusts and folds, within a Late Jurassic regional volcano-sedimentary complex (Lemaire Formation) and near the contact with overlying turbidites of the Yahgán Formation. This deposit covers rhyolite and dacite and is overlain by a complex unit composed by felsic tuff, ignimbrite and flows. The massive sulphide lens exposure is traced for over 250 m along its strike and varies from 1.5 to 4 m in thickness. Deformation is evident by a pinch-and-swell structure which splits the ore body into two portions: a pyrite-rich zone at the base that passes upwards to massive ore, and a laminated upper portion. Ore minerals include pyrite, sphalerite, chalcopyrite, galena and minor tetrahedrite and bournonite. Neither barite nor Fe oxides or chert are found within or above the massive sulphide lens. Drilling exploration indicated ore interceptions at depth with a true thickness between 3 and 18.6 m of 1 % Cu, 1.4 % Pb and 3 % Zn.

In spite of the deformation relative to a shear zone, massive sulphide ore of the Arroyo Rojo deposit retains many undeformed textures as framboids, polyframboids and banding, among others, suggesting early crystallization history. In addition, deformation, recrystallization and annealing textures are also identified. Footwall and hanging-wall felsic volcanic rocks are altered to chlorite-sericite-pyrite-quartz assemblages, being the hydrothermal alteration strongest below the orebody, where it exhibits a roughly concentric zonation with a silicic and chloritic inner zone and a sericitic external zone. Chlorite and mica compositions show systematic changes with distance from ore: from Mg-rich chlorite and phengite in proximal zones to Fe-rich chlorite and phengitic muscovite in distal areas.

In spite of previous works that classify the Arroyo Rojo deposit under the Kuroko type, that is, ore deposition from buoyant fluids forming mounds, the geological and mineralogical evidence points to a sulphide deposition in a brine pool.

Key words: volcanic-hosted massive sulphide (VMS) deposit, textures, hydrothermal alteration, brine pool, Andes, Tierra del Fuego, Argentina.

RESUMEN

El yacimiento de Arroyo Rojo, situado en las cercanías de Ushuaia, es el ejemplo más importante de sulfuros masivos polimetálicos volcánogénicos situados en el cinturón riolítico de los Andes de Tierra del Fuego. El depósito encaja en la secuencia volcanosedimentaria de la Formación Lemaire, próximo al contacto con turbiditas de la suprayacente Formación Yahgán. Todos estos materiales jurásicos se vieron afectados por pliegues y cabalgamientos con vergencia hacia el norte. En superficie, el cuerpo de sulfuros masivos se puede seguir por 250 m, su potencia oscila entre 1.5 y 4 m y se pueden diferenciar dos zonas: en la base una zona rica en pirita que gradúa hacia el techo a una zona masiva y una zona laminada. Los minerales de mena incluyen pirita, esfalerita, calcopirita y galena, y en menor proporción tetraedrita y bournonita. No aparecen barita, óxidos de hierro o jaspe, ni en el interior ni sobre el cuerpo mineralizado. Los sondeos de exploración pusieron de manifiesto la presencia de capas mineralizadas de entre 3 y 18.6 m (potencia real) de mena con las siguientes leyes: 1 % Cu, 1.4 % Pb y 3 % Zn. En el muro del depósito aparecen riolitas y dacitas y en el techo una compleja unidad constituida por tobas, ignimbritas y flujos félsicos. La deformación andina (100 – 90 Ma), evidenciada por la presencia de una zona de milonitización, divide el cuerpo mineralizado en dos partes, según una estructura de tipo acuñaamiento- engrosamiento. A pesar de la deformación mencionada, es posible encontrar texturas primarias como framboides, poliframboides y bandeados junto a texturas de recristalización y recocimiento.

Las rocas volcánicas tanto en el muro como en el techo de la mineralización están alteradas hidrotermalmente, dando lugar a una asociación clorita-sericita-pirita-cuarzo que es más penetrativa en el muro, donde muestra una zonalidad concéntrica, ocupando las zonas clorítica y silícica la parte interna y la zona sericítica, la externa. Tanto micas como cloritas muestran cambios composicionales sistemáticos conforme se alejan de la mineralización; así, se pasa de clinocloro y fengita en las zonas cercanas, y a chamosita y muscovita en las distantes.

Aunque trabajos previos incluían el depósito de Arroyo Rojo dentro del tipo Kuroko, es decir, formado por fluidos hidrotermales ascendentes que forman elevaciones sobre el fondo marino, las evidencias presentadas apuntan hacia un depósito de sulfuros de tipo “brine pool”.

Palabras clave: depósitos de sulfuros masivos volcánogénicos (VMS), texturas, alteración hidrotermal, “brine pool”, Andes, Tierra del Fuego, Argentina.

INTRODUCTION

Since Jurassic times, continental arc magmatism in the southern portion of the Andean Cordillera has produced many epithermal deposits (Schalamuk *et al.*, 1997) but few volcanic-hosted massive sulphide (VMS) deposits. Tierra del Fuego is one of the scarce places in the southern Andes where VMS mineralization may be encountered. The potential of this area to host VMS deposits was shown since the decade of 1970 and early 1980, when base metals exploration was developed by several companies (Aguilar-St. Joe 1970-72, 1980-82; Noranda 1994-96; Yamana-Polimet 1995-96; Westmin 1996-97). These efforts were mostly directed to pursue discovery of volcanic-hosted polymetallic massive sulphide deposits located in a vast rhyolitic volcanic field forming an outcrop belt (Figure 1) inboard of the Cretaceous back-arc basin. The work of the aforementioned companies outlined two regional targets: Sierra de Sorondo in the south, and Sierra de Alvear in the north (Figure 1). The first recognized massive sulphide deposit in the area was the so-called Beatriz mine (Zubia *et al.*, 1989) where a small lens of massive to semi-massive polymetallic sulphides, including cobaltite (Ametrano and Paar, 1996) was identified.

The Arroyo Rojo prospect, the main VMS mineralization in the area, is located in the Sierra de Sorondo at 54°45' S latitude and 68°06' W longitude, about 800 m a.s.l.

Although the Arroyo Rojo deposit was almost covered by a small glacier at the time of discovery in the decade of 1980, the outcrop area has increased substantially in recent years due to widespread glacier retreat in the Fuegian Andes.

Previous descriptions of Arroyo Rojo prospect have been provided by Broili *et al.* (2000) and Ametrano *et al.* (2000), who considered Arroyo Rojo as a Kuroko-type VMS deposit. Broili *et al.* (2000) also cited the results of the drilling programme (Figure 2) developed in 1997, which revealed ore interceptions at depth between 3 and 18.6 m (true thickness) with grades of 1 % Cu, 1.4 % Pb, and 3 % Zn. Additional information on petrography, mineral chemistry and hydrothermal alteration of Arroyo Rojo is found in Acevedo *et al.* (2005) and Biel *et al.* (2007).

In this contribution, we update and expand upon the geological setting and field characteristics. In particular, we focus on the major host lithologies, the types and styles of mineralization and the related hydrothermal alteration. The investigation of the mineralogy and mineral chemistry of Arroyo Rojo prospect was undertaken to (1) characterize ore mineralogy, (2) identify primary textures and their post-ore modifications, (3) determine the distribution and the composition of minerals formed during hydrothermal alteration and (4) characterize metamorphic of host lithologies and ores.

The aforementioned tasks will provide the background and context for future work focussing on interpretation of

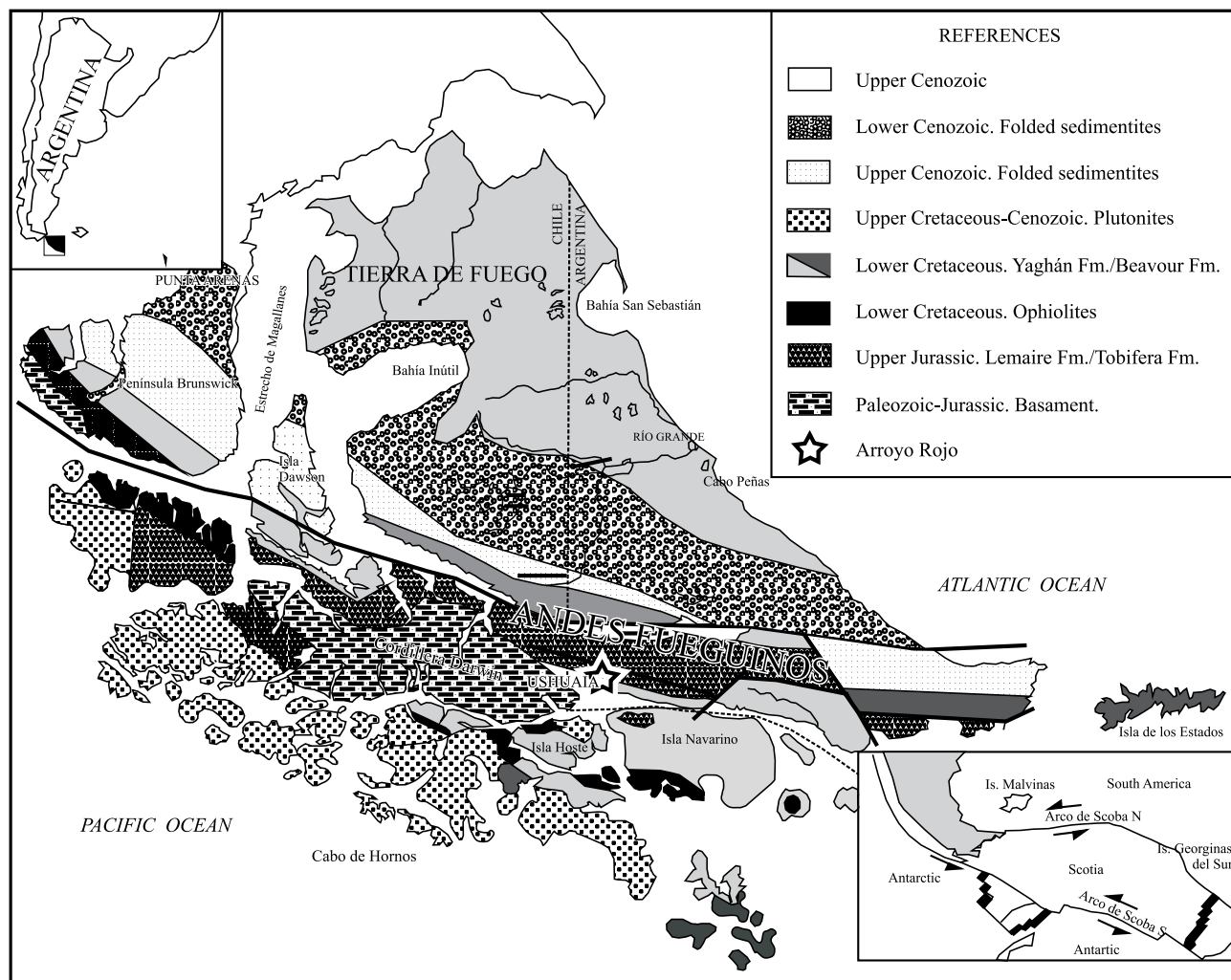


Figure 1. Geologic map of the Andes Fueguinos between 52° and 56° S, showing the location of the Arroyo Rojo volcanic-hosted massive sulphide (VHMS) deposits (modified from Olivero and Martinioni, 2001). Inset is a plate tectonic map of Tierra del Fuego (Barker, 2001).

quantitative lithogeochemical alteration studies using mass change calculations, fluid inclusion microthermometry and in situ isotope analyses, which are currently being undertaken to examine the genesis of the Arroyo Rojo deposit.

REGIONAL GEOLOGY

The Isla Grande de Tierra del Fuego (Figure 1), the largest of the Fuegian Archipelago islands, is located at the southernmost tip of South America, at 53–55° S latitude and 66–74° W longitude. The island encompasses the border between two tectonic plates: the South America and the Scotia plates separated by the Magellan Fault, where tectonic activity has been widely registered (Dalziel, 1989). The South America Plate includes middle and late Tertiary marine sedimentary rocks, which extend as high plains, isolated hills and low ranges (Rabassa *et al.*, 2000). In the Scotia Plate, the Andes of Tierra del Fuego are underlain

by an intrusive core, acid lavas and low-grade metamorphic slates. These rocks vary in age from late Paleozoic to Early Cretaceous. The southern mountainous region has been intensively eroded by late Cenozoic glaciers developing deep valleys and rugged mountains.

VMS deposits occur in the Scotia Plate and its geology is related to a succession of extensional to compressive, and transcurrent tectonic settings. Locally, three formations are recognized:

(1) the *Lapataia Formation* (pre-Jurassic, Borrelo, 1969) is considered the regional basement and consists of fine-grained phyllite with intercalations of greenstone, eruptive, basic amphibolite, and quartz-sericite and biotite-garnet schists (Caminos, 1980; Olivero and Martinioni, 2001). These rocks are so deformed that stratification is completely obliterated by schistosity and crenulation. A metamorphic peak is defined by staurolite, kyanite, and sillimanite (Dalziel and Brown, 1989). Dalziel and Cortes (1972) interpreted the aforementioned basement as an

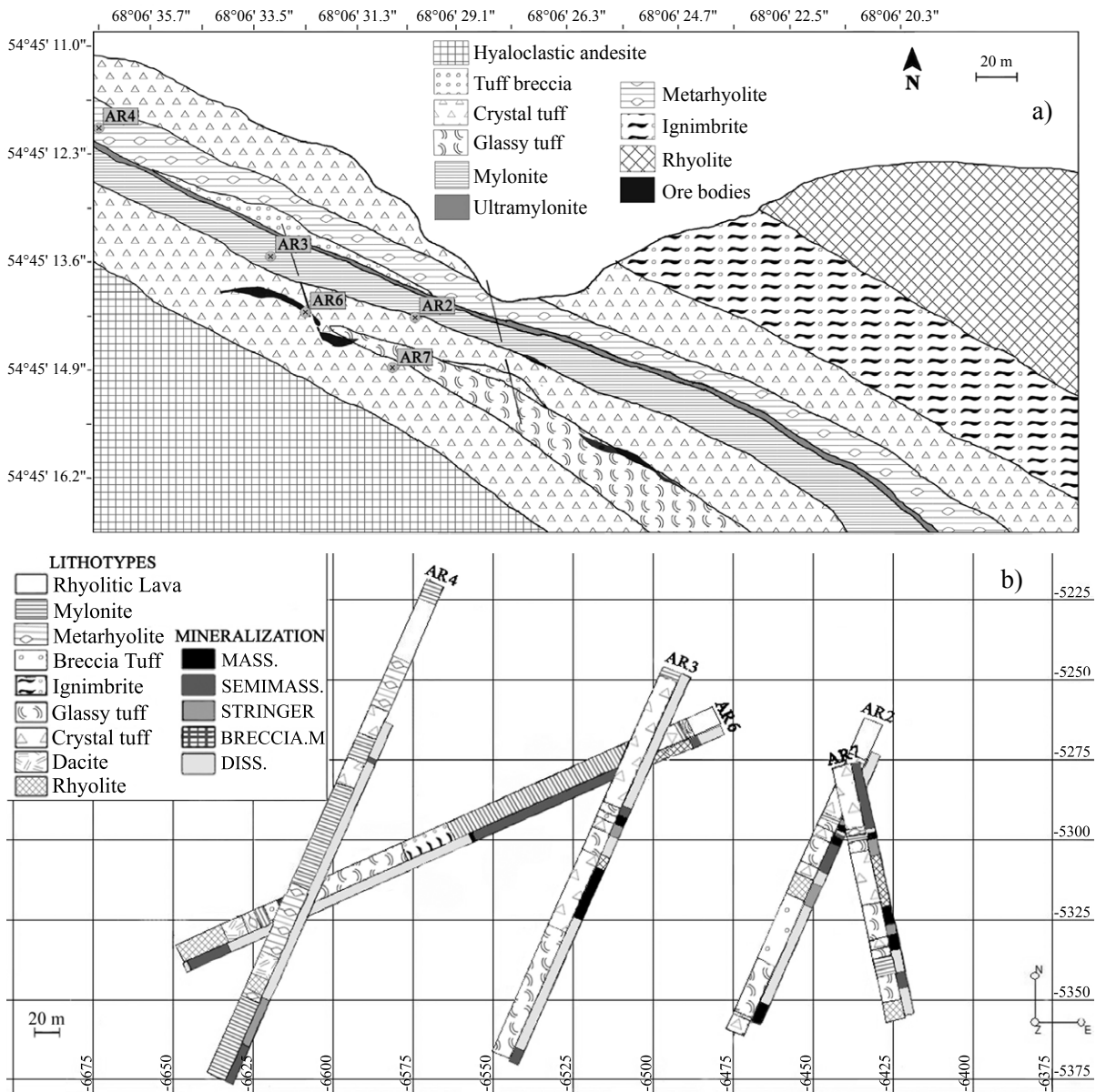


Figure 2. a) Geological map of Arroyo Rojo deposit showing the location of drill holes. Massive sulphide lenses are drawn in black; b) Drill core sketch map of Arroyo Rojo deposit, showing the relation between mineralization and lithotypes. Mineralization: mass: massive ore; semimass: semimassive ore; str: stringer; brecc m: mineralized breccia; diss: disseminated ore.

older than mid-Jurassic accretionary prism on the margin of Gondwana. The age of basement, based on isotopic and fossil data, is considered to be late Palaeozoic to Middle Jurassic (Hervé *et al.*, 1981). This basement is separated from the overlying Lemaire Formation by an angular unconformity (Kranck, 1932).

(2) the *Lemaire (Tobífera) Formation* (Late Jurassic, Kranck, 1932) consists of a basal, epiclastic member covered by volcanic and volcanoclastic acidic rocks, and intercalations of basaltic spilites. This unit is interpreted to belong to a submarine, volcano-sedimentary complex (Hanson and Wilson, 1991). These rocks are strongly deformed with a highly penetrative cleavage, which has completely obliterated the original stratification in fine-grained facies.

Hanson and Wilson (1991) pointed out a Late Jurassic age, for the Lemaire Fm. by means of isotopic and fossil data. This complex represents a deep-marine deposit formed in a volcanic-active rift, which corresponds to an embryonic stage of a back-arc marginal basin produced during regional extension related to the initial breaking-up of Gondwana (Uliana and Biddle, 1987).

(3) the *Yahgan Formation* (Early Cretaceous, Kranck, 1932) is interpreted as the volcanoclastic filling of a back-arc basin formed between the western margin of South America, and the andesitic Pacific arc (Katz, 1972; Dalziel *et al.*, 1974). These rocks are highly folded, showing tight or isoclinal folding. The age of this unit was determined by fossil identification: Tithonian-Neocomian for its basal

part and late Albian for its upper part (Aguirre-Urreta and Suárez, 1985; Olivero and Martinioni, 2001). Isotopic dating resulted in an approximated age of 68–90 Ma (Mukasa and Dalziel, 1996).

The contact between the Lemaire and Yahgan formations is dominantly tectonic, except on the less deformed areas where the contact is unconformable.

The tectonic evolution of Tierra del Fuego followed three major orogenic cycles: (a) the Gondwanian cycle that generated the basement formation, (b) the Patagonian cycle that provoked the uplifting of the Fuegian Cordillera, and (c) the Andean cycle, responsible of the Fuegian Cordillera deformation and the paleogeographic turn to its present position (Ramos, 1999). During Early to Middle Jurassic began a reactivation of Triassic rifts related to the breaking of Gondwana, originating a back-arc in the margin of Gondwana. Felsic volcanism associated to this event was interrupted by multiple marine deposition episodes. The resulting volcanic, volcanoclastic and pelagic marine deposits correspond to the Lemaire Formation. Jurassic rifting evolved into a back-arc basin, contemporary to basic volcanism that produced oceanic crust (Dalziel *et al.*, 1974). Abundant outcrops of Late Jurassic to Early Cretaceous basic pillow lava (Ophiolitic Tortuga Complex and Sarmiento Formation) are the vestiges of such oceanic floor. Synchronously, marine sedimentation in the basin originated the Springhill Formation, in proximal areas, and the Yahgan Formation, in distal ones.

The regional structure is mostly related to the Andean contractional phase responsible for the thick-skinned tectonic style, which promoted N-verging thrusts and folds systems. One of these systems constitutes the Tierra Mayor Valley that separates Sorondo and Alvear Sierras (Figure 1).

THE ARROYO ROJO DEPOSIT: GEOLOGY AND STRUCTURE

Surface geology and data obtained from five drill holes (AR2, 3, 4, 6, 7) across the Arroyo Rojo prospect (Figures 2a and b) indicate that host rocks correspond to the upper part of the Lemaire Formation and both, the host rocks and the units mapped in the immediate vicinity of the deposit correspond to the volcanic portion of this formation. Despite metamorphism and deformation, protoliths are recognizable in the study area. Our attempt is to produce a detailed stratigraphy based on the definition of lithotypes that would enhance understanding of the host rocks and facilitate mineral exploration in the district.

Local stratigraphy

The described lithotypes are divided into hanging wall and footwall with respect to the surface of the mas-

sive sulphide deposit and its host rocks. The hanging wall is composed of hyaloclastic andesite (Figure 2a) and rhyolitic lava.

(1) Rhyolitic lava has only been observed at drill cores (Figure 2b). Macroscopically this unit shows flow banding and absence of phenocrysts. Under the microscope, it contains up to 1 % of modal quartz and feldspar phenocrysts, and 5 % of vesicles filled with quartz and locally, with calcite. Glass matrix, showing flow banding, is partially to totally replaced by fine-grained quartz and sericite (Figure 3a).

(2) Tuff units host the massive sulphide mineralization. They include a wide range of volcanoclastic rocks which have been subdivided on the basis of the crystal/glass/clast proportions.

(2.1) Crystal Tuff. In hand sample, millimetric-size quartz and feldspar crystals can be recognized. Modal composition varies from 15–40 % of crystal fragments of feldspar and plagioclase to 3–10 % of crystal clasts of quartz and some feldspar. Pumice shards are present in small amounts (3–5 %) as well as titanite (1–2 %). Matrix modal content varies between 45 and 80 % and consists of fine-grained quartz and sericite with variable amounts of chlorite and calcite. In samples with less amount of crystals, glassy matrix preserved and is only partially replaced by fine-grained quartz. Pumice clasts commonly present elongated vesicles filled with chlorite and clinzoisite, polycrystalline quartz or micas, and glass is totally replaced by fine-grained chlorite-sericite or sericite-carbonate groundmass. Relict tubes and vesicles pumice shards are coated with thin sulphide mineralization. Quartz and feldspar crystals are usually fragmented and display microchannels and embayed rims filled with fine-grained quartz and sericite (Figure 3b).

(2.2) Vesicular Tuff. Macroscopically, this lithotype is marked by a high density of rounded millimetric quartz eyes, which are interpreted as infilled vesicles, and abundant quartz veinlets. Elongated vesicles are weakly aligned where incipient mylonitization appears (Figure 3c). Microscopically these rocks show abundant (20–40 %) pumice clasts, characterized by coarse-grained vesicles included in a completely chloritized, glassy matrix (Figure 3d). Vesicles are infilled with quartz, calcite and subordinate micas with a tiny pyritic envelope, (Figure 3d) and locally with radial chlorite crystals. The groundmass is recrystallized to quartz associated with sericite, chlorite and sulphides. Titanite and crystal fragments of quartz and feldspar are scarce.

(2.3) Glassy Tuff. This lithotype is characterized by glass shards with relict glassy textures, as degasification channels, perlitic texture, cusped and bubble wall shards and tube pumice clasts (Figure 3e). Locally, remnants of those textures are outlined by disseminated fine-grained, subhedral pyrite or iron oxides and locally, by micas, chlorite, and/or subrounded quartz grains. In thin section, the glassy tuff contains 20–30 % of glassy clasts, 0–10 % of pumice clasts, 5 % of secondary titanite, and less than 5

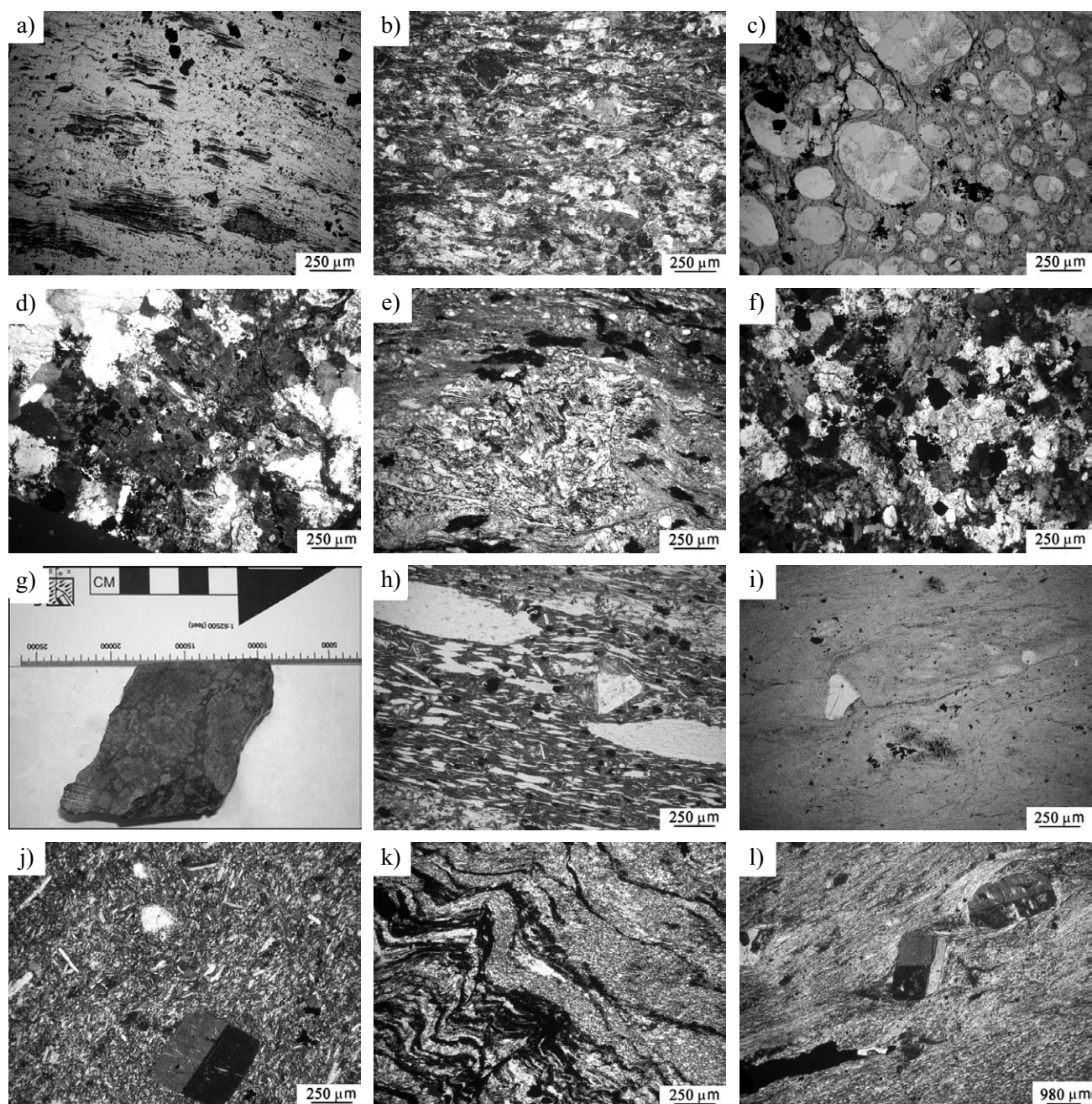


Figure 3. a) Rhyolitic lava with fluidal texture; b) Quartz and feldspar crystal fragments in a devitrified pyroclastic quartz-sericitic groundmass of a crystal tuff; c) Pumice shard with millimetric devitrified, glass vesicles and totally replaced by chlorite; d) Pumice shard replaced by chlorite in which vesicles are marked by pyritic mineralization and is partially replaced by coarse-grained quartz recrystallized tuff matrix; e) Glassy clast with degasification channels, cusped and bubble wall shards partially replaced by chlorite in a chloritic matrix of a glassy tuff; f) Glassy tuff totally devitrified and recrystallized into medium- to coarse-grained quartz, in which perlitic fractures remains are recognizable; g) Tuffaceous breccia with millimetric to centimetric altered tuff clasts in a darker quartz-pyritic matrix; h) Ignimbrite with a well developed eutaxitic texture formed by flattened strong compacted and welded of pumice lapilli in a pale brown ash matrix with presence of phenocrysts of K-feldspars, and fiammes totally replaced by chlorite; i) Some quartz phenocrysts in a poorly crystalline rhyolite; j) Na-feldspar phenocrysts and microphenocrysts in a matrix of feldspar locally replaced by quartz-sericite; k) Preferred oriented mica and quartz in two main deformational stages in milonite; l) Metarhyolite consisting of feldspar phenocrysts in an oriented quartz-micaceous matrix.

% of crystal fragments included in an abundant groundmass (60–75 %). Glass, partially to totally replaced by chlorite, or by an aggregate of fine-grained quartz-chlorite or quartz-sericite, shows fluidal textures. Locally, glassy clasts have

been nearly totally replaced by polycrystalline quartz (Figure 3f). Vesicles from pumice shards are filled with mono- and polycrystalline medium-grained quartz and chlorite. Crystal fragments of quartz and rare K-feldspar

are partially replaced by fine-grained quartz. Groundmass is recrystallized by medium- to fine-grained quartz, chlorite and subordinate sericite, and calcite.

(2.4) Brecciated Tuff. Macroscopically, it shows a well-developed brecciated texture with white millimetric to centimetric altered clasts in a dark, fine-grained groundmass (Figure 3g). Microscopically, the rock consists of crystal tuff clasts and a lesser amount of pumice clasts in a polycrystalline coarse- to medium-grained quartz matrix with mineralization and some sericite. Tuff clasts consist of sericitized, subrounded K-feldspar crystals in a quartz-sericite matrix. Pumice clasts display abundant vesicles filled with polycrystalline or monocrystalline quartz in a sericitic and feldspatic groundmass. Titanite is less abundant.

(3) Ignimbrite. Fiammes are the main macroscopic characteristic of this lithotype. Microscopically, a well developed eutaxitic texture of flattened and welded pumice lapilli in a pale brown ash matrix is observed (Figure 3h). Ignimbrite modal composition of the Arroyo Rojo deposit consists of 15–20 % fiammes, 0–15 % feldspar and quartz crystals, 0–10 % lithic clasts, 5–10 % tube pumice shards and 40–80 % groundmass. Groundmass is partially replaced by chlorite, clinozoisite and sericite. Hydrothermal titanite also occurs. Although most of fiammes are composed of chlorite without any recognizable primary internal structure, in some places a fibrous texture, subparallel to bending consisting of rare plagioclase microphenocrysts in a chloritic matrix has been observed. Lithic clasts consist of rhyolite and rare dacite.

The footwall is composed of two units:

(4) Unlike rhyolitic lava, rhyolite shows millimetric elongate quartz and K-feldspar crystals that comprise <5 % of the rock and it does not show flow banding. It may be interpreted as a dome. Microscopically, it consists of quartz and partially sericitized K-feldspar phenocrysts with some embayed rims filled with very fine-grained quartz matrix along with titanite crystals. Quartz phenocrysts are absent in those samples with less than 1–5 % phenocrysts and groundmass is totally replaced by fine-grained quartz (Figure 3i). Vesicles and veinlets filled with quartz and minor calcite are also identified.

(5) The lower unit is composed of a dacite with elongate crystals. Microscopically, this rock is composed of Na-plagioclase phenocrysts showing twinning, growth zonation and sericite alteration, and some quartz phenocrysts (Figure 3j). Phenocrysts display embayed rims replaced by fine-grained quartz. Groundmass is well preserved and consists of microphenocrysts of Na-plagioclase and some K-feldspar with flow texture. Locally, matrix is partially recrystallized to sericite, fine-grained quartz and minor chlorite.

Structure and metamorphism

Rocks in the vicinity of the Arroyo Rojo deposit experienced low-grade regional metamorphism as suggested

by the mineral associations prehnite-pumpellyite (Caminos, 1980) and chlorite-sericite-quartz-albite-epidote (Olivero and Martinioni, 2001). Recently, Biel *et al.* (2007) found that crystallinity index of micas and chlorite also suggest that the aforementioned formations reached the epizone (greenschist facies).

The Arroyo Rojo prospect is located in the core of the largest anticlinal structures and constitutes the footwall of the major stacks of the regional thrust systems. Penetrative structural fabrics are located in a shear zone associated with the main faults with the presence of mylonitic foliation. Even though foliation parallels primary layering and thrusts at regional scale, original bedding may be recognized since foliation crosses contacts between lithotypes. Likewise, massive sulphide bodies follow the primary bedding and layering, not the latter foliation. Therefore, the overall morphology of the deposit and the stratigraphic relationships between lithologic units are recognizable, even though most features of the deposit are considerably flattened and attenuated. As a consequence, both mylonite (Figure 3k) and metarhyolite (Figure 3l) are developed. A penetrative foliation, kink-bands, crenulation, S-C planes, lenticular quartz eyes and pre- and syn-kinematic titanite characterize the mylonite. The metarhyolite shows quartz and feldspar phenocrysts alignment, development of pressure shadows and secondary albitization.

Morphology of the orebodies

Mineralization at Arroyo Rojo consists of a massive sulphide lens that varies from 1.5 to 4 m in thickness, traced for over 250 m along strike and comprises pyrite and sphalerite, minor galena, chalcopyrite, and pyrrotite, and trace amounts of tetrahedrite and bournonite. Barite is not present. Deformation, evidenced by a pinch-and-swell structure, split the ore body into two portions named the upper (western) and the lower (eastern) zones (Figure 2a). Another two massive sulphide lenses have been recognized at depth (Figure 2b), which vary between 3 and 18.6 m in thickness with a trace of several meters. All the aforementioned massive sulphide bodies occur within the tuff units. From base to top, the following ore units can be observed:

(1) The footwall mineralization is exclusively pyrite, and it occurs as disseminations in a volcanic groundmass. Locally, deformation promoted mylonitization and even recrystallization, generating elongated pyrite crystals following regional foliation. Stringer veins are identified up to 5 m beneath the base of massive sulphides in both western and eastern zones. Quartz veinlets only a few millimeters to centimeters thick with subordinate pyrite, sphalerite, chalcopyrite and galena are parallel to regional foliation. These quartz-sulphide veinlets coalesce forming a lateral, metric envelope in a silicified host.

(2) A narrow (up to 0.5 m thick) zone of massive sphalerite with disseminated pyrite occurs at the base of

the ore body.

(3) Stratigraphically upwards, sulphide mineralization is dominated by sphalerite and pyrite that occurs as layered decimeter-thick intervals with distinctive composition and as massive bodies. Compositional intervals occur as millimeter-scale alternations of fine-grained pyrite and sphalerite-rich laminae. In most places, layers are parallel to the regional foliation as a result of deformation, although there are primary sedimentary features preserved in places. Massive mineralization consists of sphalerite, forming centimetric porphyroblasts and minor chalcopyrite and galena. Locally, quartz veinlets and augen-like structures have been recognized. In the upper part, there is an overall decrease of sphalerite and an increase of chalcopyrite, which occurs forming a compositional layering with pyrite, disrupted by boudinaged sphalerite porphyroblasts.

A distinct ore assemblage has been found in AR6 drill hole at 360 m depth. It consists of semi-massive pyrrhotite (50 modal %) with some euhedral, framboidal and polyframboidal pyrite and rare chalcopyrite, hosted in a dacitic matrix in which deformation and hydrothermal alteration is almost absent.

ORE MINERALOGY AND TEXTURES

Polished sections of ore samples were examined under both optical and scanning electron microscopes (SEM). Specimens were etched with HNO₃ (60 %) to develop a better definition of textural types. The composition of minerals (Table 1) was obtained by means of a Cameca SX50 electron microprobe at the University of Barcelona, with a 30 nA and a 15 kV acceleration voltage. Calibration employed both natural and synthetic mineral standards.

The composition of Arroyo Rojo pyrite, based on 225 spot analyses, corresponds to stoichiometric pyrite, which may exhibit up to 0.22 weight percent As and 0.12 weight percent Bi. Gold concentrations in all pyrite crystals are below the nominal detection limit for the instrumental conditions used.

Based on microprobe analyses, iron content in sphalerite exhibits a textural control: twinned grains contain 3.5 wt. % Fe, whereas sphalerite developing planar dislocations, shows a mean Fe content of 1.8 wt. %. This is in agreement with the textural tendency of twinned grains to host chalcopyrite inclusions. Tetrahedrite has Ag contents between 3.2 and 6.7 wt. % and Zn contents between 1.7 and 1.9 wt. %. Based on microprobe data (Table 1), galena, pyrrhotite and chalcopyrite are characterized by stoichiometric proportions of the major components and by the presence of Bi as minor component.

Primary textures

At first sight the only evidence for primary sulphide deposition is framboidal pyrite observed in the layered ore. However, HNO₃ etching of aggregates and isolated crystals reveals numerous framboidal (Figure 4a), colloform (Figure 4b) and euhedral relict cores. These textures indicate primary depositional textures. A few euhedral grains show growth zonation forming a concentric pattern of inclusions (Figure 4c). Acid etching has also shown that most of the framboids are polyframboidal (Love, 1971) or groups of radial pyrite crystals (Figure 4d).

Although sphalerite, chalcopyrite and pyrrhotite are less competent than pyrite and consequently growth microstructures are usually obliterated by deformation and

Table 1. Average compositions of the main ore minerals of Arroyo Rojo from microprobe analyses.

| | Pyrrhotite (n=25) | | Galena (n=33) | | Sphalerite (n=92) | | Chalcopyrite (n=54) | | Pyrite (n=225) | |
|--------------|-------------------|--------|---------------|-------|-------------------|-------|---------------------|-------|----------------|-------|
| | Med. | S.D. | Med. | S.D. | Med. | S.D. | Med. | S.D. | Med. | S.D. |
| wt. % | | | | | | | | | | |
| S | 37.79 | ±0.73 | 13.27 | ±0.23 | 33.04 | ±0.50 | 34.32 | ±0.82 | 52.72 | ±1.08 |
| Zn | 0.00 | ±0.00 | 0.00 | ±0.00 | 63.09 | ±1.45 | 0.00 | ±0.00 | 0.00 | ±0.00 |
| Pb | 0.00 | ±0.00 | 85.63 | ±1.01 | 0.00 | ±0.00 | 0.00 | ±0.00 | 0.00 | ±0.00 |
| Fe | 59.40 | ±1.03 | 0.02 | ±0.03 | 2.99 | ±0.92 | 29.78 | ±0.42 | 46.28 | ±0.60 |
| Cu | 0.02 | ±0.04 | 0.05 | ±0.05 | 0.07 | ±0.15 | 34.32 | ±0.59 | 0.04 | ±0.31 |
| Co | 0.10 | ±0.05 | 0.00 | ±0.00 | 0.00 | ±0.00 | 0.03 | ±0.03 | 0.06 | ±0.04 |
| Ni | 0.07 | ±0.04 | 0.00 | ±0.00 | 0.00 | ±0.00 | 0.04 | ±0.06 | 0.04 | ±0.06 |
| Mn | 0.00 | ±0.00 | 0.00 | ±0.00 | 0.15 | ±0.05 | 0.00 | ±0.00 | 0.00 | ±0.00 |
| As | 0.00 | ±0.02 | 0.07 | ±0.07 | 0.01 | ±0.02 | 0.01 | ±0.02 | 0.22 | ±0.63 |
| Ag | 0.04 | ±0.03 | 0.08 | ±0.10 | 0.00 | ±0.00 | 0.02 | ±0.03 | 0.02 | ±0.03 |
| Cd | 0.00 | ±0.00 | 0.06 | ±0.09 | 0.21 | ±0.06 | 0.00 | ±0.00 | 0.00 | ±0.00 |
| Sb | 0.00 | ±0.00 | 0.03 | ±0.04 | 0.00 | ±0.00 | 0.00 | ±0.00 | 0.00 | ±0.00 |
| Bi | 0.10 | ±0.09 | 0.11 | ±0.14 | 0.00 | ±0.00 | 0.08 | ±0.08 | 0.12 | ±0.11 |
| Hg | 0.00 | ±0.00 | 0.00 | ±0.00 | 0.07 | ±0.13 | 0.00 | ±0.00 | 0.00 | ±0.00 |
| Total | 97.51 | ±19.15 | 99.54 | ±1.19 | 99.64 | ±0.77 | 98.60 | ±0.74 | 99.50 | ±1.17 |

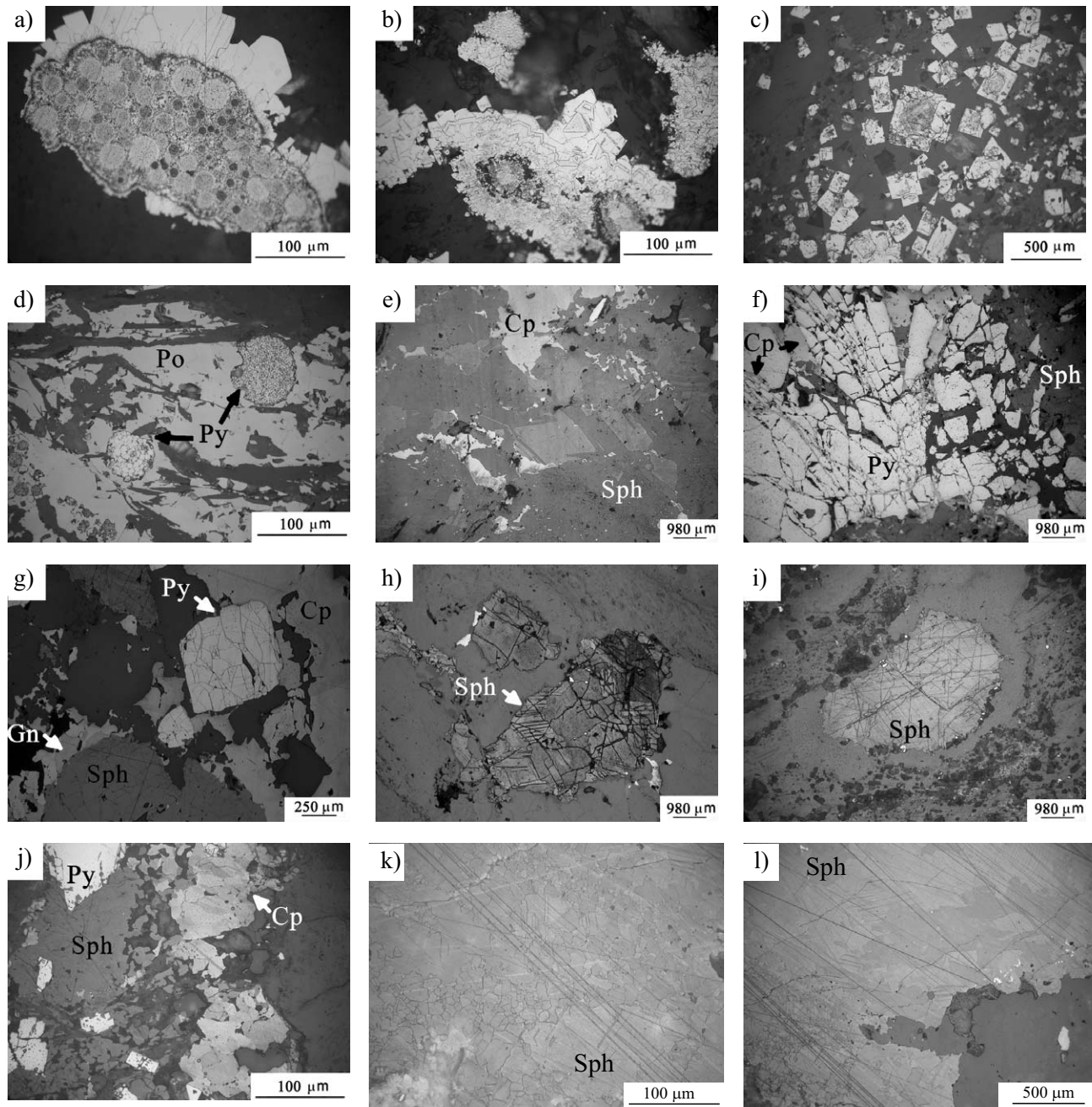


Figure 4. a) Euhedral pyritic radial overgrowths over polyframboidal cores; b) Colloform overgrowth over framboidal core; c) Growing zonation in pyritic crystals d) Polyframboids consisting of individual euhedral crystals; e) Growing twinning in sphalerite oblique to chalcopyrite disease, f) Oriented fractures in pyrite with incipient developing of cataclastic flow; g) Oriented planar dislocations in euhedral pyritic crystal; h) Deformational twins in sphalerite with poor-developed chalcopyrite disease; i) Developing of a high-density dislocations reticulate in a coarse sphalerite grain; j) Growing twinning in chalcopyrite; k) Annealing twins developed in triple junctions of recrystallized grains; l) Coarse sphalerite grains with deformational twins and fine-grained recrystallization on the rims. Key: Sph: sphalerite, Cp: chalcopyrite, Py: pyrite, Gn: galena, Po: pyrrotite.

recrystallization, a few primary textures have been preserved. Abundant, broad, laminar and low-density growth twins in the sense of Frater (1985a) are preserved in coarser sphalerite grains (Figure 4e). Moreover, chalcopyrite displays a weak development of broad parallel-side twins that may be considered growing twins according to criteria of Cox and Etheridge (1984).

Deformation textures

Brittle failure is the dominant mechanism of deformation in pyrite, due to its hardness and generally refractory nature (Vokes, 1969). Pyrite porphyroclasts at Arroyo Rojo are generally cracked and microfractured, aligned to preferred or aleatory orientations and filling

ductile phases (gangue minerals, sphalerite, chalcopyrite and galena) by plastic injection (Figure 4f). Intense brittle deformation locally results in an important grain-size reduction (cataclastic texture). The rigidity of pyrite porphyroclasts is also manifested by pressure shadows of quartz, chlorite and muscovite. Locally, sphalerite porphyroclasts also develop pressure shadows, mainly of fibrous quartz.

Pyrite elongation parallel to regional foliation has been observed in mylonites. According to Cook *et al.* (1993), this texture is due to a pressure solution mechanism, which is common in chlorite-biotite. Pressure solution is also important in the metamorphic deformation of pyrite, as evident with the presence of indentation and sutured grain boundaries. This mechanism is possibly responsible of delicate overgrowths on relict cores of the aforementioned primary textures (Brown and McClay, 1993). Finally, pyrite also shows evidence of ductility as support lattice dislocations suggested by the alignment of etch pits forming subgrains walls that indicate the onset of polygonization (Figure 4g).

Deformation textures in sphalerite and chalcopyrite are evident by twinning (Figures 4h and 4j) and dislocations lattices accompanied (Figure 4i), in some cases, by development of subgrains.

Galena exhibits the most ductile behaviour of the sulphide association; its softness is responsible of the removing of the microstructures by etching. In spite of that, galena locally displays abundant lattice dislocations indicating an incipient granoblastic recrystallization.

Recrystallization textures

As aforementioned, mineralization experienced deformation and metamorphism and consequently, recrystallization and annealing textures are present in sphalerite and minor galena and pyrite. According to Brown and McClay (1993) pyrite has a tendency to recrystallize under low-grade metamorphic conditions. Pyrite displays heterometric, granoblastic mosaics of fine-grained recrystallized grains with triple junctions near 120°. Galena and pyrrhotite also show triple junctions in polygonal grains of granoblastic textures in zones where etching has not completely obliterated relicts of the primary textures (Frater, 1985b; Pesquera and Velasco, 1993). Sphalerite etching revealed a broad, well-developed polygonal recrystallization to finer grain with triple junctions (Figure 4k). Within these grains numerous parallel-sided twins can be interpreted as annealing twins (Frater, 1985b). Locally, recrystallized grains surround coarse grains with deformational twins or lattice dislocations with abundant annealing twinning (Figure 4l), as those described by Brill (1989). According to these authors, the previously mentioned microfabric is the consequence of dislocation creep flow as a mechanism of deformation.

HYDROTHERMAL ALTERATION

Hydrothermally altered rocks are found predominantly in the immediate footwall of the massive sulphide mineralization, defining a roughly concentric zonation, with an inner silicic and chloritic zone and an external sericitic zone. Silicification is mainly found within the sulphide zones, showing highly variable concentrations. Chloritization, only developed in the footwall, is observed both within the mineralized zones and in surrounding host rocks. Sericitization is pervasive and typically better developed within the surrounding host rocks, extending beyond the chloritic zone. In most drill holes, there is a gradual transition from chlorite to sericite zones with increasing distance from the massive sulphide lens.

(1) Silica alteration is characterized by the pervasive development of quartz in rocks at the top of massive sulphide mineralization. This alteration type defines narrow zones within rhyolite and includes quartz veins with pyrite and sphalerite, ranging up to 3 cm in width.

(2) Chlorite alteration zone is characterized by abundant chlorite replacing felsic volcanoclastic rocks. The result is a dark green, chloritized rock with moderate to coarsely flattened, felsic volcanic rock fragments. In Arroyo Rojo, chlorite is common beneath the massive sulphide bodies. Under the microscope, it occurs as fine- to coarse-grained aggregates and locally, fill cracks. Based on electron probe microanalyzer results, chlorite closer to the sulphide lenses (clinocllore) are enriched in Mg (6.3–9.2 atoms per formula unit- a.p.f.u.) and depleted in Fe (0.3–2.6 a.p.f.u.) relative to distal chlorite (chamosite), which shows a variable Fe content between 2.3 and 4.9 a.p.f.u., reaching their K content up to 0.3 a.p.f.u (Table 2). This latter chlorite forms compact, flakes aggregates, which locally have a radial texture. As it can be seen in Figure 5a, there is a transition between the aforementioned chlorite compositions. In addition, chlorite also occurs as fringes or halos accompanying pressure shadows developed on pyrite and sphalerite crystals in both, massive sulphide and disseminated mineralization with Fe-compositional range between 0.4 and 0.7 a.p.f.u..

(3) Sericitization is the most extensive and widespread alteration zone. It is characterized by moderate to pervasive development of sericite in felsic volcanoclastic rocks throughout the deposit, both within, below, and lateral to (or outboard of) the zone of chlorite alteration, but occurs most commonly in the footwall of massive sulphides. Sericite-altered rocks are intensely foliated. It should be noted that it is difficult, in places, to distinguish hydrothermal sericite alteration from that formed in felsic rocks in response to regional metamorphism and deformation, particularly where the former is only weakly developed. Under the microscope, sericite occurs as fine-grained aggregates partially to totally replacing both K-feldspars and the volcanic groundmass along with quartz and scarce carbonates, as coarse-grained aggregates within massive sulphide and forming pressure shadows in relation to disseminated pyrite crystals in the

Table 2. Electron probe microanalyses of chlorite in the related hydrothermal alteration of the Arroyo Rojo deposit.

| | Chlorite | | | | | | | |
|------------------------------------|------------------|--------|-------|------|--------------------|--------|-------|------|
| | Distal (n = 100) | | | | Proximal (n = 143) | | | |
| | Min. | Max. | Med. | S.D. | Min. | Max. | Med. | S.D. |
| <i>wt. %</i> | | | | | | | | |
| SiO₂ | 24.01 | 32.76 | 27.57 | 1.99 | 27.30 | 36.68 | 31.09 | 1.61 |
| TiO₂ | 0.00 | 0.08 | 0.02 | 0.02 | 0.00 | 1.93 | 0.03 | 0.16 |
| Al₂O₃ | 14.15 | 22.63 | 19.62 | 1.46 | 15.39 | 21.43 | 18.76 | 1.13 |
| FeO | 11.30 | 27.08 | 20.44 | 4.85 | 2.35 | 18.98 | 6.31 | 4.20 |
| MnO | 0.00 | 0.58 | 0.20 | 0.19 | 0.14 | 0.65 | 0.39 | 0.11 |
| MgO | 11.04 | 25.96 | 18.58 | 3.74 | 17.36 | 33.05 | 28.95 | 3.26 |
| CaO | 0.00 | 0.75 | 0.07 | 0.09 | 0.00 | 1.48 | 0.06 | 0.13 |
| Na₂O | 0.00 | 0.10 | 0.02 | 0.02 | 0.00 | 0.27 | 0.01 | 0.03 |
| K₂O | 0.00 | 1.87 | 0.15 | 0.36 | 0.00 | 2.26 | 0.10 | 0.26 |
| Total | 94.87 | 102.17 | 98.24 | 1.34 | 94.69 | 102.04 | 98.07 | 1.49 |
| <i>a.p.f.u.</i> | | | | | | | | |
| Si | 2.62 | 3.23 | 2.86 | 0.14 | 2.79 | 3.41 | 3.02 | 0.11 |
| Ti | 0.00 | 0.01 | 0.00 | 0.00 | 0.00 | 0.15 | 0.00 | 0.01 |
| Al/Al^{IV} | 0.77 | 1.38 | 1.14 | 0.14 | 0.59 | 1.21 | 0.98 | 0.11 |
| Al^{VI} | 0.89 | 1.84 | 1.26 | 0.14 | 0.90 | 1.63 | 1.16 | 0.08 |
| Fe | 0.92 | 2.45 | 1.78 | 0.47 | 0.18 | 1.58 | 0.52 | 0.36 |
| Mg | 1.70 | 3.87 | 2.86 | 0.52 | 2.54 | 4.64 | 4.18 | 0.41 |
| Mn | 0.00 | 0.05 | 0.02 | 0.02 | 0.01 | 0.06 | 0.03 | 0.01 |
| Ca | 0.00 | 0.08 | 0.01 | 0.01 | 0.00 | 0.16 | 0.01 | 0.01 |
| Na | 0.00 | 0.02 | 0.00 | 0.00 | 0.00 | 0.05 | 0.00 | 0.01 |
| K | 0.00 | 0.24 | 0.02 | 0.05 | 0.00 | 0.28 | 0.01 | 0.03 |

Normalized to O₁₀(OH)₈.

footwall. Chemical composition of sericite (Table 3) is controlled by their spatial position relative to mineralization: proximal sericite is marked by (Fe+Mg) ratios between 0.34 to 0.67 a.p.f.u., while distal ones vary from 0.19 to 0.42 a.p.f.u. Thus, mica composition varies from phengite to phengitic muscovite (Figure 5b). It is worth noting that Ba content can be as high as 0.03 a.p.f.u..

GENETIC CONSIDERATIONS

Discussions on the conditions and mechanisms of deposit of massive sulphide on the sea floor have resulted in two scenarios (*e.g.* Solomon *et al.*, 2004 and Tornos and Heinrich, 2008): ore deposition from buoyant fluids forming mounds (*black smoker*) and from saline fluids in sea floor depressions (*brine pool model*). Previous works of Arroyo Rojo deposit are believed to follow the widely extended Kuroko model (Broili *et al.*, 2000; Ametrano *et al.*, 2000; Acevedo *et al.*, 2005) but the present study reveals that the features described in preceding sections point to deposition in a brine pool.

Arroyo Rojo deposit is the largest polymetallic massive sulphide deposit in the Tierra del Fuego rhyolitic belt, displaying several mineralized lenses and high ratio features (maximum length/average thickness, Solomon *et*

al., 2004). The host rocks of the deposit are felsic volcanic and volcanoclastic rocks. Mineralization consists of pyrite, sphalerite and lesser amounts of galena and chalcopyrite and rare pyrrhotite and tetrahedrite and bournonite, and shows no-systematic variation in sphalerite composition. Many textures of the early stages of crystallization are still preserved in spite of subsequent deformation and metamorphism; acid etching revealed the existence of framboids and polyframboids, and also delicate colloform and radial overgrowths. Near the top of the ore body, centimeter-scale pyritic laminae alternate with sphalerite-(galena) rich laminae. The lamination formed previously to cleavage and it may be the result of sedimentation and winnowing. Likewise, lack of evidence for ore deposition by replacement, presence of albite, lack of barite and Fe-oxides and no significant change in FeS content of sphalerite passing from the massive sulphide lenses, also suggest deposition in a brine pool. Additionally, no feeder conduits or chimney fragments such as seen at Hellyer (Solomon *et al.*, 2004), have been found. Based on our field observations, the fluid

Table 3. Electron probe microanalyses of sericite in the related hydrothermal alteration of the Arroyo Rojo deposit.

| | Sericite | | | | | | | |
|------------------------------------|-----------------|--------|-------|------|-------------------|--------|-------|------|
| | Distal (n = 21) | | | | Proximal (n = 50) | | | |
| | Min. | Max. | Med. | S.D. | Min. | Max. | Med. | S.D. |
| <i>wt. %</i> | | | | | | | | |
| SiO₂ | 45.48 | 59.16 | 49.68 | 3.22 | 47.19 | 58.95 | 50.24 | 1.88 |
| TiO₂ | 0.00 | 1.54 | 0.11 | 0.32 | 0.00 | 0.19 | 0.05 | 0.04 |
| Al₂O₃ | 20.96 | 33.24 | 30.53 | 3.10 | 22.72 | 30.94 | 28.83 | 1.60 |
| FeO | 0.23 | 2.66 | 0.70 | 0.57 | 0.19 | 2.00 | 0.60 | 0.34 |
| MnO | 0.00 | 0.08 | 0.01 | 0.02 | 0.00 | 0.07 | 0.02 | 0.02 |
| MgO | 1.69 | 3.68 | 2.45 | 0.56 | 2.87 | 6.07 | 3.97 | 1.02 |
| CaO | 0.00 | 1.40 | 0.10 | 0.29 | 0.00 | 0.12 | 0.02 | 0.03 |
| Na₂O | 0.14 | 0.44 | 0.26 | 0.10 | 0.00 | 0.35 | 0.12 | 0.07 |
| K₂O | 7.42 | 10.60 | 9.83 | 0.71 | 8.83 | 11.05 | 10.42 | 0.43 |
| BaO | 0.00 | 1.10 | 0.48 | 0.38 | 0.00 | 0.77 | 0.37 | 0.20 |
| H₂O(c) | 4.26 | 4.65 | 4.49 | 0.10 | 4.30 | 4.72 | 4.49 | 0.08 |
| Total | 93.93 | 102.03 | 98.63 | 2.13 | 95.12 | 102.43 | 99.13 | 1.48 |
| <i>a.p.f.u.</i> | | | | | | | | |
| Si | 3.15 | 3.97 | 3.32 | 0.19 | 3.26 | 3.747 | 3.35 | 0.08 |
| Ti | 0.00 | 0.08 | 0.01 | 0.02 | 0 | 0.01 | 0 | 0 |
| Al/Al^{IV} | 0.03 | 0.85 | 0.68 | 0.19 | 0.25 | 0.744 | 0.65 | 0.08 |
| Al^{VI} | 1.52 | 1.82 | 1.73 | 0.08 | 1.45 | 1.704 | 1.62 | 0.07 |
| Fe²⁺ | 0.01 | 0.15 | 0.04 | 0.03 | 0.01 | 0.113 | 0.03 | 0.02 |
| Mn²⁺ | 0.00 | 0.00 | 0.00 | 0.00 | 0 | 0.004 | 0 | 0 |
| Mg | 0.17 | 0.37 | 0.24 | 0.05 | 0.29 | 0.612 | 0.39 | 0.1 |
| Ca | 0.00 | 0.10 | 0.01 | 0.02 | 0 | 0.009 | 0 | 0 |
| Na | 0.02 | 0.06 | 0.03 | 0.01 | 0 | 0.047 | 0.02 | 0.01 |
| K | 0.63 | 0.89 | 0.84 | 0.06 | 0.77 | 0.94 | 0.89 | 0.04 |
| Ba | 0.00 | 0.03 | 0.01 | 0.01 | 0 | 0.02 | 0.01 | 0.01 |
| Sum Cat | 8.54 | 8.99 | 8.91 | 0.10 | 8.77 | 9.06 | 8.96 | 0.05 |
| X_{Mg} | 0.30 | 0.47 | 0.44 | 0.04 | 0.36 | 0.487 | 0.46 | 0.03 |
| Oct | 1.85 | 2.08 | 2.02 | 0.06 | 1.96 | 2.149 | 2.05 | 0.04 |
| Int | 0.69 | 0.94 | 0.89 | 0.06 | 0.77 | 0.983 | 0.91 | 0.04 |

Normalized to O₁₀(OH)₈.

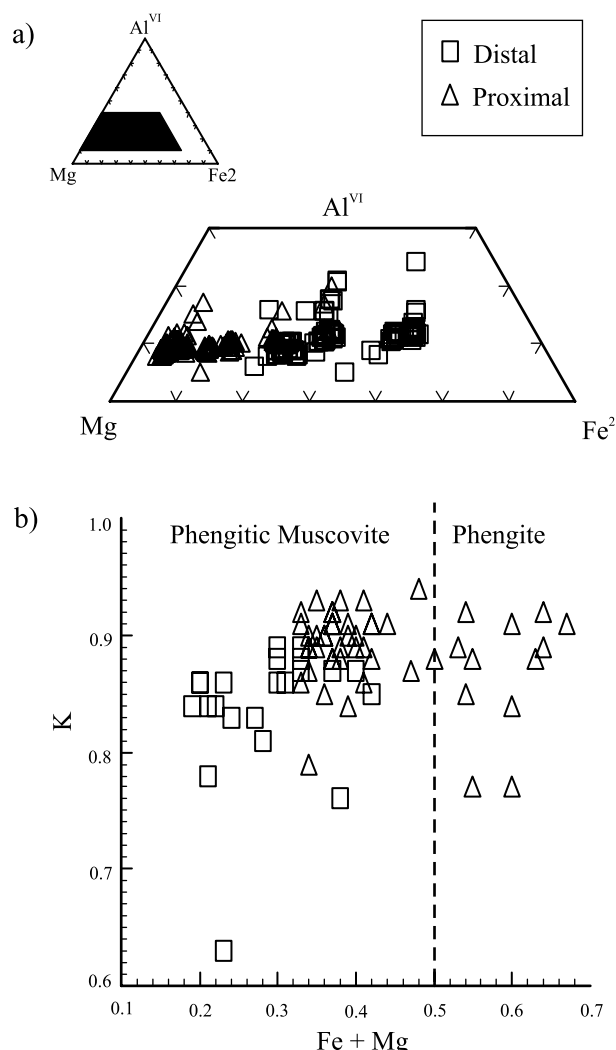


Figure 5. a) Al^{VI} -Mg-Fe cation plot showing trend of Mg-rich chlorite with distance to the Arroyo Rojo deposit; b) K vs. (Fe+Mg) showing trend of phengite with distance to the Arroyo Rojo deposit.

sources possibly lie outside the mineralized zone, within the Lago Guanaco prospect that is stratigraphically lower than Arroyo Rojo deposit and can be interpreted as a feeder zone since it consists of quartz-sulphide stringer veins, which may channel fluids that precipitated massive sulphides. Preliminary *in situ* (Fallick *et al.*, 1992) $\delta^{34}S$ values in sulphides range from slightly positive to very negative $\delta^{34}S$ values (-27.5 to +2.3 ‰), but most of them are in the -20 to +1 per mil range. There is no vertical variation in $\delta^{34}S$ values through Arroyo Rojo deposit. Sulphur isotopic data indicate a contribution of both biologically reduced sulphur production from seawater sulphate and deep-seated sulphur that also fits well in a brine pool model.

Regarding hydrothermal alteration, the composition of chlorite and mica was found to vary with distance to ore at Arroyo Rojo, displaying a broad shift from Mg-rich chlorite and phengite in proximal zones to Fe-rich chlorite and phengitic muscovite in distal areas. However, this al-

teration pattern is not typical of VMS deposits: in general high Fe-chlorite is associated with mineralization. Jones *et al.* (2005) described a similar situation at Myra Falls Camp (British Columbia, Canada). This unusual distribution prevents us to apply hydrothermal alteration criterion as a tracer of deposition model.

To sum up, most of the aforementioned Arroyo Rojo features lead us to suggest ore formation in a brine pool according to the criteria of Solomon *et al.* (2004).

ACKNOWLEDGEMENTS

The study of the Arroyo Rojo VMS deposit is part of the project: "The massive sulphides of Tierra del Fuego: mineral deposit modelling and geological criteria for ore exploration", funded by Dirección General de Programas y Transferencia de Conocimiento (DGPTC) del Ministerio de Ciencia e Innovación (MICINN). We gratefully acknowledge the Dirección General de Recursos Mineros de la provincia de Tierra del Fuego, which provided access to drill holes. The Grupo de Recursos Minerales is supported by Gobierno de Aragón. We are also grateful to Dr. Bissig and Dr. Canet for their constructive reviews of the manuscript.

REFERENCES

- Acevedo, R.D., Fanlo, I., Subías, I., Paniagua, A., Buffone, D.E., 2005, Polymetallic VMS deposits of the Andes Fuegoinos (southernmost Argentina): Preliminary report, in Mao, J., Bierlein, F.P. (eds.), Mineral Deposit Research: Meeting the Global Challenge: Berlin, Springer, 599-602.
- Aguirre-Urreta, M.B., Suárez, M.D., 1985, Belemnites de la secuencia turbidítica volcanoclástica de la Formación Yahgán, Titiocretácico inferior del extremo sur de Chile, in IV Congreso Geológico Chileno, Antofagasta, Chile: Actas, 1, 1-16.
- Ametrano, S., Paar, W.H., 1996, La composición química de los sulfuros de mina Beatriz, Tierra del Fuego: un aporte para su interpretación metalogénica, in 13º Congreso Geológico Argentino y 3º Congreso de Exploración de Hidrocarburos, 3, 159-172.
- Ametrano, S., Etcheverry, R., Echebest, H., Godeas, M., Zubia, M., 2000, VMS district of Tierra del Fuego, Argentina, in Sherlock, R., Logan, M.A.V. (eds.), VMS Deposits of Latin America: Geological Association of Canada, Ontario, 593-612.
- Barker, P.F., 2001, Scotia Sea regional tectonic evolution: implication for mantle flow and palaeocirculation: Earth Science Reviews, 55, 1-39.
- Biel, C., Subías, I., Fanlo, I., Mateo, E., Acevedo, R.D., 2007, Styles, mineralogy and textures of the Arroyo Rojo polymetallic massive sulphide prospect, Tierra del Fuego (Argentina), in Andrew, C.J. (ed.), Digging Deeper: Proceedings of the Ninth Biennial SGA Meeting, Dublin, Ireland: Society for Geology Applied to Mineral Deposits, 1081-1084.
- Borrelo, A.V., 1969, Los geosinclinales de la Argentina: Dirección Nacional de Geología y Minería, Anales, 14, 1-118.
- Brill, B., 1989, Deformation and recrystallization microstructures in deformed ores from the CSA mine, Cobar, N.S.W., Australia: Journal of Structural Geology, 11(5), 591-601.
- Broili, C., Klohn, M., Odre, R.W., 2000, Exploration, Geology and mineral deposits in the Fin del Mundo project, Tierra del Fuego, Argentina, in Sherlock, R., Logan, M.A.V. (eds.), VMS Deposits of Latin

- America: Ontario, Geological Association of Canada, 567-591.
- Brown, D., McClay, K.R., 1993, Deformation textures in pyrite from the Vangorda Pb-Zn-Ag deposit, Yukon, Canada: *Mineralogical Magazine*, 57, 67-81.
- Caminos, R., 1980, Cordillera Fueguina, in Turner, J.C.M. (coord.), Segundo Simposio de Geología Regional Argentina: Academia Nacional de Ciencias, Córdoba, 1463-1501.
- Cook, N.J., Halls, C., Boyle, A.P., 1993, Deformation and metamorphism of massive sulphides at Sulitjema, Norway: *Mineralogical Magazine*, 57, 67-81.
- Cox, S.F., Etheridge, M.A., 1984, Deformation microfabric development in chalcopyrite in fault zones, Mt. Lyell, Tasmania: *Journal of Structural Geology*, 6(1-2), 167-182.
- Dalziel, I.W.D., 1989, Tectonics of the Scotia Arc, Antarctica, Field trip Guide, Vol. T180: Washington, D. C., American Geophysical Union, 206 pp.
- Dalziel, I.W.D., Brown, R.L., 1989, Tectonic Denudation of the Darwin Metamorphic Core Complex in the Andes of Tierra-Del-Fuego, Southernmost Chile - Implications for Cordilleran Orogenesis: *Geology*, 17, 699-703.
- Dalziel, I.W.D., Cortes, R., 1972, Tectonic style of southernmost Andes and the Antartides, in XXIV International Geological Congress, Montreal, 3, 316-327.
- Dalziel, I.W.D., Dewit, M.J., Palmer, K.F., 1974, Fossil Marginal Basin in Southern Andes: *Nature*, 250, 291-294.
- Fallick, A.E., McConville, P., Boyce, A.J., Burgess, R., Kelley, S.P., 1992, Laser microprobe stable isotope measurements on geological materials: some experimental considerations (with special reference to $\delta^{34}\text{S}$ in sulphides): *Chemical Geology*, 101, 53-61.
- Frater, K.M., 1985a, Mineralization at the Golden Grove Cu-Zn deposit, Western Australia I: Premetamorphic textures of the opaque minerals: *Canadian Journal of Earth Sciences*, 22, 1-14.
- Frater, K.M., 1985b, Mineralization at the Golden Grove Cu-Zn deposit, Western Australia II: Deformation textures of the opaque minerals: *Canadian Journal of Earth Sciences*, 22, 15-26.
- Hanson, R.E., Wilson, T.J., 1991, Submarine rhyolitic volcanism in a Jurassic proto-marginal basin; southern Andes, Chile and Argentina, in Harmon, R.S., Rapela, C.W. (eds.), Andean magmatism and its tectonic setting: Boulder, Colorado, Geological Society of America, 13-27.
- Hervé, F., Nelson, E., Kawashita, K., Suárez M., 1981, New Isotopic Ages and the Timing of Orogenic Events in the Cordillera Darwin, Southernmost Chilean Andes: *Earth and Planetary Science Letters* 55, 257-265.
- Jones, S., Herrmann, W., Gemmell, J.B., 2005, Short Wavelength Infrared Spectral Characteristics of the HW Horizon: Implications for Exploration in the Myra Falls Volcanic-Hosted Massive Sulfide Camp, Vancouver Island, British Columbia, Canada: *Economic Geology*, 100, 273-294.
- Katz, H.R., 1972, Plate tectonics and orogenic belts in the South-east Pacific: *Nature*, 237, 331-332.
- Kranck, E.H., 1932, Geological investigations in the Cordillera of Tierra del Fuego: *Acta Geographica*, 4, 1-231.
- Love, L.G., 1971, Early diagenetic polyframboidal pyrite, primary and redeposited, from the Wenlockian Denbigh Grit Group, Conway, North Wales, U. K.: *Journal of Sedimentary Petrology*, 41(4), 1038-1044.
- Mukasa, S.B., Dalziel, I.W.D., 1996, Southernmost Andes and South Georgia Island, North Scotia Ridge: Zircon U-Pb and muscovite Ar-40/Ar-39 age constraints on tectonic evolution of Southwestern Gondwanaland: *Journal of South American Earth Sciences*, 9, 349-365.
- Olivero, E.B., Martinioni, D. R., 2001, A review of the geology of the Argentinian Fuegian Andes: *Journal of South American Earth Sciences*, 14, 175-188.
- Pesquera, A., Velasco, F., 1993, Ore metamorphism in sulfide mineralizations from the Cinco Villas Massif (Western Pyrenees, Spain): *Economic Geology*, 88, 266-282.
- Rabassa, J., Coronato, A., Bujalesky, G., Salemme, M., Roig, C., Meglioli, A., Heusser, C., Gordillo, S., Roig, F., Borromei, A., Quattrocchio, M., 2000, Quaternary of Tierra del Fuego, Southernmost South America: an updated review: *Quaternary International*, 68-71: 217-240.
- Ramos, V.A., 1999, Rasgos estructurales del territorio argentino. 1. Evolución tectónica de la Geología Argentina, Capítulo 24: Buenos Aires, Argentina, Universidad de Buenos Aires, Facultad de Ciencias Exactas y Naturales, Departamento de Ciencias Geológicas, Laboratorio de Tectónica Andina, *Anales* 29(24), 715-784.
- Schalamuk, I.B., Zubia, M., Genini, A., Fernández, R.R., 1997, Jurassic epithermal Au-Ag deposits of Patagonia, Argentina: *Ore Geology Reviews*, 12, 173-186.
- Solomon, M., Tornos, F., Large, R.R., Badham, J.N.P., Both, R.A., Zaw, K., 2004, Zn-Pb-Cu volcanic-hosted massive sulphide deposits: criteria for distinguishing brine pool-type from black smoker-type sulphide deposition: *Ore Geology Reviews*, 25, 259-283.
- Tornos, F., Heinrich, C.A., 2008, Shale basins, sulfur-deficient ore brines and the formation of exhalative base metal deposits: *Chemical Geology*, 247, 195-207.
- Uliana, M.A., Biddle, K.T., 1987, Permian to late Cenozoic evolution of northern Patagonia: main tectonic events, magmatic activity and depositional trends, in Mackenzie, G.D. (ed.), *Gondwana Six: structure, tectonics and geophysics*: American Geophysical Union, *Geophysical Monograph*, 40, 271-286.
- Vokes, F.M., 1969, A review of the metamorphism of sulphide deposits: *Earth Sciences Reviews*, 5, 99-143.
- Zubia, M., Godeas, M., Ametrano, S., 1989, Area mina Beatriz, Territorio Nacional del Tierra del Fuego, República Argentina: una manifestación de metales de base estratoligada y singenética, in Brodtkorb M., Schalamuk, I., (eds.), *Simposios sobre el Cretácico de América Latina IGCP 242, C15-C44*.

Manuscript received: May 25, 2009

Corrected manuscript received: October 15, 2009

Manuscript accepted: December 8, 2009